

# Efficient Premature Ventricular Contraction Detection based on Network Dynamics Features

Yumin Shen<sup>1,†</sup>, Zhipeng Cai<sup>1,†</sup>, *Member, IEEE*, Li Zhang<sup>2</sup>, *Senior Member, IEEE*, Bor-Shyh Lin<sup>3</sup>, *Senior Member, IEEE*, Jianqing Li<sup>1,\*</sup>, *Member, IEEE*, Chengyu Liu<sup>1,\*</sup>, *Senior Member, IEEE*

**Abstract**—Automatic detection of premature ventricular contractions (PVCs) is essential for early identification of cardiovascular abnormalities and reduction of clinical workload. As the most prevalent arrhythmia, PVCs can cause cardiac failure or sudden death. The difficulty resides in extracting features that effectively reflect the electrocardiogram (ECG) signals. Transition networks (TN), which represent the transition relationships between various phases of a time series, are advantageous for capturing temporal dynamics. Therefore, in order to recognize PVCs, each heartbeat was firstly split into several segments; then their statistical properties were calculated for the sequence construction; finally, network topology related features were extracted from TN constructed by these sequences of statistical properties, and input into decision trees-based Gentleboost for PVC recognition. The algorithm was trained on MIT-BIH arrhythmia database (MIT-BIH-AR), and tested on St. Petersburg Institute of Cardiological Technics 12-lead arrhythmia database (INCART), wearable ECG database (WECG), and noise stress test database by four evaluation metrics: sensitivity, positive predictivity, F1-score (F1) and area under the curve (AUC). The proposed algorithm achieved an average F1 of 0.9784 and AUC of 0.9975 on MIT-BIH-AR, and proved good generalization ability on INCART and WECG with F1=0.9633 and 0.9467, AUC=0.9887 and 0.9755, respectively. The algorithm also exhibited robustness and noise immunity as evidenced by tests on sensitivity of R-wave peak offset and noise, and real-world daily life conditions. Overall, the proposed PVC detection algorithm based on TN theory offered high classification accuracy, strong robustness, and good generalization ability, with great potential for wearable mobile applications.

**Index Terms**—Electrocardiogram (ECG), Dynamic ECGs, Premature ventricular contractions, Transition network, Wearable.

## I. INTRODUCTION

Public health has long focused on cardiovascular disease

This research was funded by the National Natural Science Foundation of China (62171123, 62001105, 62071241), the National Key Research and Development Program of China (2022YFC2405600, 2023YFC3603600), the China Postdoctoral Science Foundation (2023M730585), the Jiangsu Funding Program for Excellent Postdoctoral Talent (2023ZB812).

Yumin Shen, Zhipeng Cai, Jianqing Li and Chengyu Liu are with the State Key Laboratory of Digital Medical Engineering, School of Instrument Science and Engineering, Southeast University, Nanjing 210096, China (e-mails: 220213661@seu.edu.cn; zhipeng@seu.edu.cn; lj@seu.edu.cn; chengyu@seu.edu.cn).

Li Zhang is with the Department of Computer Science, Royal Holloway, University of London, Surrey TW20 0EX, UK (e-mail: li.zhang@rhul.ac.uk).

Bor-Shyh Lin is with the Institute of Imaging and Biomedical Photonics, National Chiao Tung University, Hsinchu 30010, Taiwan (e-mail: borsyhlin@gmail.com).

<sup>†</sup>Yumin Shen and <sup>†</sup>Zhipeng Cai have the equal contribution to this work.

\*Jianqing Li and Chengyu Liu are the corresponding authors (e-mails: lj@seu.edu.cn and chengyu@seu.edu.cn).

(CVD), which caused more than 17 million deaths globally in 2019, or 32% of global mortality, according to World Health Organization [1]. Cardiac arrhythmias, which are a prevalent type of CVD, refer to irregular heartbeats resulting from disorders in either the heart's origin or conduction pathways. These abnormalities can lead to sudden death and cardiac collapse due to excessive strain on the heart [2, 3]. As the most common cardiac arrhythmia, premature ventricular contractions (PVCs), originating in the ventricles of the heart, are often characterized by atypical QRS complexes with widened morphology in the electrocardiogram (ECG). PVCs have significant prognostic implications as they elevate the risk of heart failure, malignant arrhythmias, and sudden cardiac death [4]. Meanwhile, they can occur both in individuals without underlying cardiac conditions and those with pre-existing heart disease, with their prevalence reaching up to 75% during 24-hour or 48-hour ambulatory ECG monitoring [4, 5]. Clinicians typically detect PVCs by observing changes in heart rhythm and subtle morphological variations in ECG signals, which can be greatly simplified by automated ECG signal analysis, especially for long-term dynamic ECG records.

Automated ECG signal analysis involves preprocessing, heartbeat segmentation, feature extraction, and classification. Classification outcomes heavily depend on proper feature extraction. There are two types of methods for extracting ECG signal features: deep learning-based automatic feature extraction and handcrafted feature extraction. Deep learning methods can extract and classify information automatically and has become popular in the healthcare applications. Peng et al. [6] utilized Convolutional Neural Network (CNN) and sequence-to-sequence model with attention mechanism based on bidirectional Long Short-Term Memory (LSTM) for a 5-class classification including PVC on MIT-BIH Arrhythmia database (MIT-BIH-AR). Their model achieved an accuracy of 0.9928 and an F1-score (F1) of 0.957, with the only drawback being the large amount of training time and data required. Similarly, Hou et al. [7] utilized LSTM-based auto-encoder network to extract ECG signal features for the classification of 5 heartbeat types, achieving the average accuracy and sensitivity (Se) of 0.9974 and 0.9935. Meng et al. [8] proposed a CNN model for wearable ECG classification and tested it on their own database with comparable performance. Although deep learning has great accuracy in ECG arrhythmia classification, the aforementioned research still struggles with computational complexity. In addition, deep learning's black box nature makes it difficult to apply to high-risk decisions like cardiac diagnosis [9].

&gt; &lt;

Handcrafted features include morphological, statistical and wavelet features. Morphological characteristics are the most intuitive and extensively used features for PVC detection, as arrhythmias always present as simple alterations in ECG waveform. The most prominent waveform (P-QRS-T complex) in ECG determines its morphological representation: amplitude, duration, and area. M. Hammad et al. [10] extracted 13 morphological features, such as amplitude and duration of the QRS complex, for ECG signal classification. Their computationally efficient algorithm obtained an overall accuracy of 0.99 on MIT-BIH-AR, relying heavily on ECG signal quality and the accuracy of fiducial point detection. Sokolova et al. [11] proposed a rule-based PVC detection algorithm using heart rhythm and 6 different QRS shape metrics, achieving 0.827 Se and 0.8297 positive predictivity (P+) on MIT-BIH-AR. Interestingly, the combination of traditional morphological features and features extracted by other analysis methods could achieve enhanced classification performance. Chen et al. [12] combined ECG P-QRS-T segment morphological features with principal component analysis (PCA) and dynamic time warping algorithm (DTW) attributes to classify arrhythmias. Their approach achieved an accuracy rate of 0.978. Raj et al. [13] selected RR-interval features and extracted morphological features through discrete orthogonal stockwell transform and PCA for multiple arrhythmia classification including PVC, obtaining the overall accuracy, Se and P+ of 0.9882, but with a long computational time. Allami et al. [14] incorporated 3 morphological and 7 statistical parameters into the Cascade Forward Neural Network (CFNN) for PVC identification, but their model lacked anti-noise testing in noisy environments.

Owing to the intricate nature of the cardiac system and the nonlinearity exhibited by ECG signals, an increasing number of studies have incorporated nonlinear analysis techniques into healthcare applications. In recent years, nonlinear time series analysis has notably employed complex network-based methodologies, which have emerged as a significant research area. Complex networks serve as a powerful tool for revealing interdependencies among elements within a system. In this context, nodes in the network represent the elements under consideration, and edges represent their interrelationships. When applied to time series analysis, the nodes and edges of a network typically represent distinct data points or patterns derived from the time series, along with their temporal associations [15]. The fundamental concept involves mapping time series data onto complex networks and subsequently quantifying the dynamics of the time series using various topological statistics. Three principal approaches for mapping time series onto complex networks are proximity networks, visibility graphs, and transition networks [16-18]. Among these approaches, transition networks stand out as their nodes correspond to restricted discrete states (patterns) within the time series, with connections based on temporal transitions between these states (patterns). Transition networks primarily describe the transition relationships and nonlinear dynamic behavior among the states (patterns), thus retaining sufficient

temporal information to effectively capture the dynamic characteristics in the sequence. Therefore, the ECG signals were analyzed from the perspective of transition networks in this study. Several studies have demonstrated the effectiveness of transition networks in accurately capturing the dynamics of time series, particularly in distinguishing ECG signal segments in different health conditions. Parlitz et al. [16] used ordinal pattern statistics and symbolic dynamics to differentiate congestive heart failure patients from healthy individuals. McCullough et al. [17] devised an ordinal pattern network based on order patterns derived from relative magnitudes in fixed-length time series, successfully distinguishing ECG segments related to normal sinus rhythm, ventricular tachycardia, and ventricular fibrillation. Weng et al. [18] utilized a transition network to discriminate between healthy and pathological conditions in the human heart system.

In conventional feature-based methods mentioned above, widely used features, such as width, amplitude, and area, are typically extracted from multiple segments based on identified fiducial points. These features aim to capture the variations in the ECG waveform within a single heartbeat [10, 12, 14]. However, these extracted features heavily rely on a highly precise P-QRS-T detection algorithm and focus primarily on limited pre-defined linear information. Consequently, they may overlook potential hidden information and nonlinear relationships present in the data. In contrast, transition networks are constructed by tracking the succession of states over time, enabling a more straightforward capture of the dynamic temporal characteristics exhibited by time series data. To fully explore the dynamic characteristics of ECG signals, a new feature extraction method and detection algorithm for PVC recognition based on the theory of transition networks was proposed. Specifically, the statistical properties of each intra-beat segment are mapped into transition networks, allowing for the extraction of topological statistics to aid in PVC identification. As transition networks inherently maintain the temporal information within a heartbeat, the resulting topological statistics serve as representations of the network structure that can effectively reflect the nonlinear dynamic properties inherent in ECG signals.

This paper introduces a novel application of transition networks for beat-to-beat heartbeat classification in ECG signal analysis, expanding upon existing network-related studies. The main objective and challenging problem addressed in this research is to determine an appropriate method for mapping the ECG waveform onto transition networks while ensuring that the networks retain sufficient information to effectively capture the dynamics of the original signals. The proposed classification algorithm adopts a computationally efficient approach, employing the static symbolic encoding method to discretize the sequences of statistical properties extracted from the ECG waveform. Within this method, the node in transition networks is defined by sequential patterns formed by multiple consecutive symbols. This choice of symbolic encoding offers several advantages, including reduced sensitivity to noise and

&gt;&lt;

enhanced interpretability, as the sequential patterns and their interrelationships closely align with the underlying characteristics of the ECG waveform. The proposed algorithm was trained on MIT-BIH-AR and tested on the St. Petersburg Institute of Cardiological Technics 12-lead arrhythmia database (INCART) and the wearable ECG database (WECG). In addition, cross-database experiments were performed to assess the algorithm's robustness against noise and its dependence on accurate R-wave peak detection. The main contribution of this study can be outlined as follows:

- (1) From the perspective of transition networks, an efficient feature extraction method was proposed that can extract novel good-interpretable features reflecting complex nonlinear dynamics from the ECG signals.
- (2) A novel network feature-based algorithm for PVC detection was proposed, leveraging dynamic properties for classification using an ensemble learner, validated on multiple databases with outstanding classification performance and generalizability.
- (3) The noise test and R-peak offset test were conducted, demonstrating good noise immunity and R-wave offset immunity.
- (4) The application of transition networks is expanded to the classification of beat-to-beat arrhythmias, beyond the classification of ECG data segments.

The rest of this paper is organized as follows. Section II presents the description of the database used. The methodology of this study is presented in Section III. Detailed results of all the experiments are presented in Section IV. Finally, discussions and conclusions are drawn in Sections V and VI, respectively.

## II. MATERIAL

### A. MIT-BIH-AR Database

The MIT-BIH-AR Database [19] comprises 48 half-hour records of ECG signals. These records were collected by the BIH Arrhythmia Laboratory between 1975 and 1979. Each record consists of two channels, specifically modified-lead II along with one of the following leads: V1, V2, V4, or V5. The database includes data obtained from a total of 47 subjects. All records were sampled at 360 Hz within 10 mV range. In this study, the modified-lead II ECG signals were resampled to 400 Hz and used for analysis and model evaluation. Four records containing paced beats (102, 104, 107 and 217) had been excluded from the experiments according to the AAMI recommendation [20]. Training and testing ECG signals were taken from the remaining data. The beats used in the experiments were 81,249 beats, consisting of 74,360 normal beats (N) and 6,889 PVCs, which were summarized in Table I.

### B. INCART Database

The St. Petersburg Institute of Cardiological Technics 12-lead arrhythmia database (INCART) [19] is composed of 75 half-hour annotated records obtained from 32 Holter records. The data was collected from a total of 17 men and 15 women, ranging from 18 to 80 years old. The signals were sampled at a

frequency of 257 Hz. In this study, the lead II ECG signals were resampled to 400 Hz and used for testing, including 168,004 beats (148,364 N and 19,640 PVCs).

### C. Wearable ECG Database

The wearable ECG database (WECG) is a collection of ECG records obtained using the wearable 12-lead ECG SmartVest system [21]. It encompasses 5 three-hour records of lead-II ECG signals, collected from 5 volunteers between the ages of 26 and 65, all with a history of PVCs. The ECG signals were digitized at a sampling rate of 400 Hz. Within the WECG database, there were a total of 66,150 beats that were annotated and labeled by two independent cardiology experts. These annotations include the location of the R-peak (the highest point on the QRS complex) for each beat, as well as the type label indicating whether the beat is N or a PVC. In terms of the beat types, there are 58,326 N and 7,824 PVCs within the database. It is worth noting that all records in the WECG database were collected in daily life environments, ensuring high-quality dynamic data that could closely reflect the performance in practical applications. Similarly, in order to further assess the classification performance in daily applications, the ECG dataset during daily activities was collected from 10 participants, including 5 healthy adults and 5 individuals with non-fatal frequent PVCs, during sitting, talking, walking (3 km/h) and jogging (5 km/h). Participants were requested to perform a single activity to ensure their consistent activity throughout the entire recording period. The ECG dataset during daily activities consisted of 49,668 beats (47,381 N and 2,287 PVCs), including 40 approximately 15-min ECG records from each participant during four different daily activities. The patient experimental protocols (Reference code: 2020-SRFA-183) had been approved by the Ethics Committee of The First Affiliated Hospital of Nanjing Medical University.

### D. Noise Stress Test Database

To explore the robustness against physiological ECG signal noise, three typical types of ambulatory ECG noise from MIT-BIH Noise Stress Test Database (MIT-BIH-NST) [19] were added to wearable ECG database to construct the noise stress test samples for noise testing. Three half-hour records of noise in ambulatory ECG, namely baseline wander (bw), muscle artifact (ma) and electrode motion artifact (em), were resampled at 400 Hz and linearly combined to form the fourth

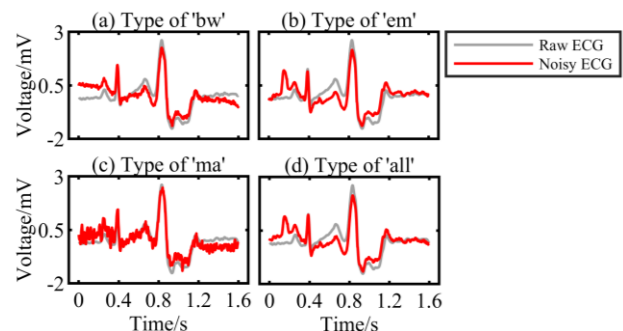


Fig. 1. Four types of noisy ECG signals generated by adding noise from MIT-BIH-NST (SNR = 6dB), with raw signal in grey for comparison.

&gt; &lt;

TABLE I  
THE LIST OF THE DATABASES

	Database	# Total beats	# N beats	# V beats	
Train	MIT-BIH-AR	81,249	74,360	6,889	
	INCART	168,004	148,364	19,640	
	WECCG	66,150	58,326	7,824	
Test	MIT-BIH-NST	66,150	58,326	7,824	
					bw
					ma
					em
	Daily life ECG dataset	49,668	47,381	2,287	

# means the number of the beats.

noise type (all) in the noise stress test database, as shown in Fig. 1. Before adding noise to the ECG database, the existing physiological noise signals were removed as much as possible by a band-pass filter (0.1-45Hz) and isoline correction. Each noise signal was added to each ECG record in wearable ECG database without interruption by temporal periodic repetition at a specific signal-to-noise ratio (SNR). The SNR was chosen as 18dB, 9dB, 6dB and 3dB respectively.

### III. METHOD

In this paper, the proposed PVC recognition algorithm consists of four main steps (Fig. 2): (1) ECG preprocessing and segmentation, (2) mapping the ECG waveform to transition networks, (3) network-based effective feature extraction and (4) heartbeat classification with an ensemble classifier.

#### A. Preprocessing and segmentation

ECG signals are inherently weak electrophysiological signals that are susceptible to interference and noise due to the complexity of the human body. Therefore, preprocessing of ECG signals is necessary to reduce the impact of various artifacts such as baseline wander and muscle interference. To exclude baseline drift and high-frequency noise, a Butterworth band-pass (0.1-45 Hz) filter was applied. Then, Pan-Tompkin's algorithm [22] was employed for R-wave peak detection in each ECG record. Based on the detected R-wave peak locations, a window of 0.5 s duration was used to segment the heartbeat. This window spanned 0.1 s before and 0.4 s after the R-wave peak, capturing the relevant waveform information for further analysis [23].

#### B. Transition network construction

##### 1) Extraction of statistical properties for each heartbeat

The ECG signal is characterized by quasi-periodic behavior, exhibiting similarities across different cardiac cycles. This property allows for the identification of dynamic changes within a single heartbeat, providing valuable information for classification. In order to capture the dynamic morphological changes within a heartbeat, each heartbeat waveform was divided into several segments. Then, several statistical features were calculated from each segment, including morphological positive/negative area, energy, mean value, average rectified value, and root mean square. By calculating these statistical

features for different intra-beat segments, it becomes possible to observe the changing patterns of the feature sequences. These changing patterns contain dynamic information that can be effectively utilized for heartbeat classification.

Morphological positive/negative area: Wave-area-based characteristics are acceptable for defining heartbeat morphology due to the relevance of waveform fluctuation during the cardiac cycle. The positive area is the region above baseline surrounded by ECG wave and baseline, whereas the negative area is the region below baseline.

Energy: Signal energy measures ECG signal power. It shows ECG signal amplitude for each cardiac cycle segment. Signal energy sequences match cardiac cycle stages. Signal energy in a single segment is calculated as (1), using  $x(p)$  to represent the intra-beat segment with N points.

$$En = \sum_{p=1}^N x^2(p) \quad (1)$$

Mean value: Mean value shows the intra-segment ECG signal's central tendency or usual value. The mean value sequence is the down-sampled ECG signal with just the average amplitude in each intra-beat segment. Its computation method is,

$$AVG = \sum_{p=1}^N x(p) / N \quad (2)$$

Average rectified value (ARV): ARV measures the average magnitude of the rectified waveform after eliminating signal polarity. It shows the average ECG signal strength, including positive and negative deflections. Its calculation formula is,

$$ARV = \sum_{p=1}^N |x(p)| / N \quad (3)$$

Root mean square (RMS): The signal's root mean square indicates its power transmission capability. It is the square root of the average of the squared ECG signal values, calculated as follows,

$$RMS = \sum_{p=1}^N \sqrt{x^2(p)} / N \quad (4)$$

##### 2) Symbolic encoding statistical properties as symbol sequences

The nodes in a transition network are restricted discrete states. However, the initial statistical properties have too many possibilities in terms of numerical values, so they cannot be directly used for network construction. Therefore, proper discretization of the sequence and definition of nodes and edges in the network are crucial in the conversion to network representation. Symbolic encoding has been widely used to discretize the sequence with continuous distribution. Generally, there is considerable freedom in the definition of symbols for the time series. Static encoding, also called coarse-graining of phase space, discretizes the sequence based on the absolute amplitude of the data value via a set of pre-defined thresholds. Compared to dynamic encoding, which focuses more on the differences between data values, the choice of static encoding was made to preserve the wide and enlarged morphological characteristics of the PVC beat. Moreover, as a coarse-graining process, symbol coding reduces the sensitivity of the algorithm to noise and enhances the robustness of the algorithm [24].

Based on the threshold values  $\{thr_1, thr_2, \dots, thr_{K-1}\}$ , static

&gt;&gt;

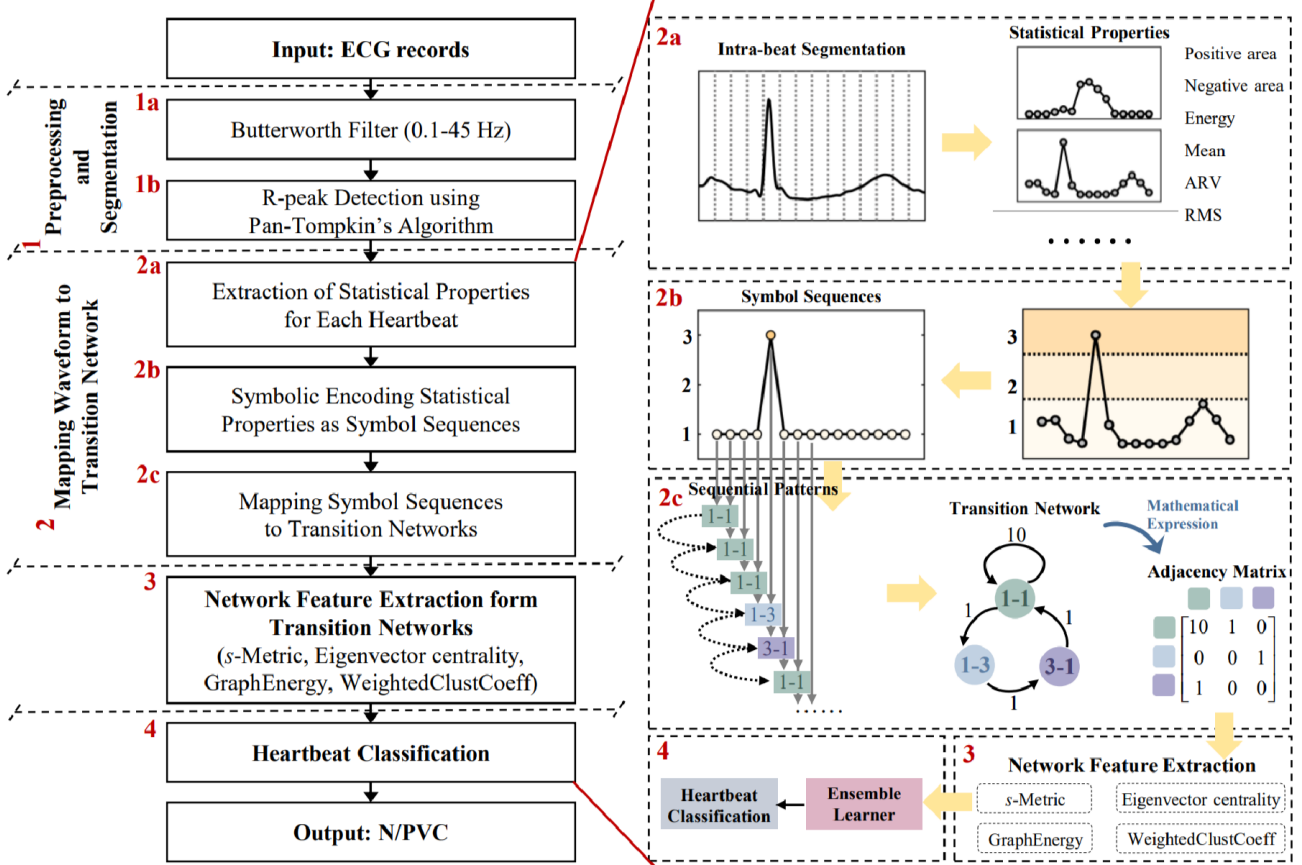


**Fig. 2.** Flow chart of the proposed PVC classification algorithm, with a detailed schematic representation on the right corresponding to steps in the flow chart labeled the same marker. The number of the discrete symbol  $K$  was set to 3 and the length of the sequential sequence  $m$  was set to 2, thereby the resulting network with  $3^2=9$  different nodes. Note that only the nodes occurred have been drawn in the schematic representation and a simplified matrix has replaced the original  $9 \times 9$  adjacency matrix.

encoding converts the data series into  $K$  discrete symbols. Specifically, equation (5) demonstrates the conversion of the sequence of statistical property  $\{f_i\}_{i=1}^N$  to the coarse-grained symbol sequence  $\{s_i\}_{i=1}^N$ . A combination of the research theory and experimentation was used to determine the most optimum parameter  $K$  in static encoding. Previous studies [25] suggest a much smaller number of  $K < 5$  for nonlinear time series analysis based on transition networks. Based on the experimental results, after balancing the classification performance and run time,  $K$  was finally set equal to 3. Therefore, threshold values  $\{thr_1, thr_2\}$  transformed feature sequences to 3 discrete symbol sequences.

$$s_i = \begin{cases} N & thr_{K-1} \leq f_i \\ \dots & \dots \\ 2 & thr_1 \leq f_i < thr_2 \\ 1 & f_i < thr_1 \end{cases} \quad (5)$$

### 3) Mapping symbol sequences to transition networks

The next critical step is the construction of transition networks. There are different types of definition for network nodes and edges. As for coarse-graining based transition networks, the simplest way to define a network node is that every suitable defined symbol is naturally regarded as a node, which is suitable for investigating the significance of single symbol. Another common definition of a node is the ordinal

pattern, which is the rank order of observations in the time series according to their relative magnitudes. However, the ordinal pattern only captures the segment shapes without the magnitude. In order to obtain more structured information and better identify the patterns in the time series, the sequential patterns formed by multiple consecutive symbols are considered as network nodes, their temporal transitions determine the connections between the nodes.

For the node, the coarse-grained sequence  $\{s_i\}_{i=1}^N$  is progressively partitioned to yield the series of sequential patterns  $\{v_i\}_{i=1}^{N-m+1}$ , where  $v_i = (s_i, s_{i+1}, \dots, s_{i+m-1})$  and  $m$  is the length of sequential pattern. There are  $K^m$  different patterns in the series of sequential patterns  $\{v_i\}_{i=1}^{N-m+1}$ , which also indicates  $K^m$  different nodes in the network. In particular, when  $m = 2$ , a vector of two successive symbols is considered as a node  $\gamma_i = (s_i, s_{i+1})$ , thus the network should have  $K^2$  nodes. For the edge, the connections between network nodes should reflect the temporal behavior of sequential patterns, thereby depending on the temporal order of these patterns. In addition, the weight of the edge is proportional to the times of transitions between the two patterns. More specifically, the edges in the network depend on the series of sequential patterns  $\{v_i\}_{i=1}^{N-m+1}$ , thus an edge between two nodes implies that their sequential patterns are adjacent.

According to the aforementioned steps, a directed and

&gt; &lt;

weighted network  $G$  can be expressed mathematically in the form of a  $n \times n$  adjacency matrix  $A=(a_{ij})_{1 \leq i, j \leq n}$ , with nonzero value or zero in position  $(i, j)$  according to whether node  $i$  connects to node  $j$  or not. For a weighted adjacency matrix,  $a_{ij}=w_{ij}$  when node  $i$  connects to node  $j$  with the weight  $w_{ij}$ , while for an unweighted network, there are only 1 and 0 in the matrix. By using the matrix representation of the network, the network properties can be calculated more easily by applying basic concepts from linear algebra.

### C. Network-based feature extraction

Through the previous two steps, networks with adequate temporal information have the potential to capture effective features of dynamic properties. Transition networks formed by different heartbeat types have various topologies, indicating the different arrangement of nodes and edges in the network. Network properties, particularly topological properties, can help us to extract meaningful information revealing the relationship between the relevant sub-structures. Thus,  $s$ -Metric, graph energy, eigenvector centrality, and weighted clustering coefficient were employed to measure network topology, among which the degree was widely used in computation of these topological properties. The degree of a network node is the number of edges that connect to a node, expressed as  $d_i$  for node  $i$  as shown in (6).

$$d_i = \sum_{k=1}^n a_{ik} \quad (6)$$

The description of topological properties used in this study are as follows.

$s$ -Metric: To distinguish the network with same node set and similar degree distribution,  $s$ -Metric [26] is defined as the sum of products of nodal degrees across all edges as shown in (7), where  $i$  and  $j$  represent nodes connected by an edge,  $d_i$  represents the degree of node  $i$ , and  $d_j$  represents the degree of node  $j$ . Higher  $s$ -Metric value indicates stronger degree correlation, characterized by high-degree nodes connecting to other high-degree nodes and low-degree nodes connecting to other low-degree nodes. Conversely, lower  $s$ -Metric values suggest a more random or less correlated degree distribution in the network.

$$s\text{-Metric} = \sum d_i d_j \quad (7)$$

GraphEnergy: The graph energy [27], denoted as  $E(G)$ , is defined as the sum of the absolute values of the eigenvalues of the adjacency matrix, which represents node connections in the network. It can be represented as (8), where  $\lambda_i$  is the eigenvalue. The graph energy numerically quantifies the overall connectivity of the graph representation of the ECG feature sequences.

$$E(G) = \sum |\lambda_i| \quad (8)$$

Eigenvector centrality: When measuring the centrality of one node, both the number and the centrality of the adjacent nodes need to be taken into account. Hence, the eigenvector centrality [28] is proposed as the positive multiple of the sum of adjacent centralities as shown in (9), which is proportional to the sum of the centrality scores of its adjacent nodes  $c(j)$ , weighted by the strength of their connections  $a_{ij}$  and the max

eigenvalue of the adjacent matrix  $\lambda_{max}$ . For the same number of the adjacent nodes, the more important the adjacent nodes are, the higher the eigenvector centrality of that node.

$$c(i) = \lambda_{max}^{-1} \sum a_{ij} c(j) \quad (9)$$

WeightedClustCoeff: Weighted clustering coefficient [29] is a measure that balances topological information with the weight distribution information in a network, which combines both the connectivity of nodes and the weights assigned to their connections. It can be expressed as (10), where  $d_i$  and  $d_i^w$  represent the degree of node  $i$  in the network without weight and with weight respectively. Then the sum part of (10) considers all possible pairs of its neighbors and calculates a similarity or proximity measure that combines the weight of the edge with the connectivity of the node, where  $j, k$  are the possible pair in the network,  $w_{ij}, w_{ik}$  are the weight of the connecting edge, and  $a_{ij}, a_{ik}$  are the element in adjacent matrix.

$$c_i^w = 1 / d_i^w (d_i - 1) \sum (w_{ij} + w_{ik}) a_{ij} a_{ik} a_{jk} / 2 \quad (10)$$

### D. Heartbeat classification

Class imbalance affects classification learning outcomes since the ratio of N to PVC is about 11:1 in MIT-BIH-AR database. Lu et al. [30] employed numerous common strategies to balance the dataset, but Random Over Sampler (ROS) was the most successful method. In this study, ROS was adopted to tackle the imbalanced class distribution problem by increasing sample sizes of the minority class to equalize N and PVC in the training set [30].

For supervised classification in particular, the ensemble learner is a powerful combination of multiple weak learners. A primary advantage of the ensemble learner is that the defects of a single learner are likely to be compensated by the performance of the other learners, resulting in improved prediction accuracy. In this investigation, the ensemble learner Gentleboost was constructed using decision trees as weak learners. Gentleboost is a well-known ensemble method with the benefits of rapid convergence and output of real values [31]. For  $x_i$  corresponding to training sample  $i$  with the label  $y_i$  and weight  $w_i$ , the principle of the Gentleboost algorithm is [32]: the weights of each training sample are initially equalized; a regression function is fitted for each iteration based on weighted least squares of  $y_i$  to  $x_i$  with weights  $w_i$ ; the weights  $w_i$  are then updated using the equation  $w_i = w_i \exp(-y_i f_m(x_i))$  and renormalized such that  $\sum w_i = 1$ . The ultimate classifier is a linear combination of all regression functions.

### E. Evaluation methods

Sensitivity (Se), positive predictivity (P+), F1-score (F1) and area under the curve (AUC) were used to evaluate classifier performance. AUC is defined as the area under the curve ROC, which indicates the ability to distinguish between the positive and negative beats. TP, FP, TN, and FN denote true positives, false positives, true negatives, and false negatives, respectively. Statistic parameters are defined below.

$$Se = \frac{TP}{TP + FN} \quad (11)$$

&gt;&gt;

$$P_+ = \frac{TP}{TP + FP} \quad (12)$$

$$F1 = \frac{2TP}{2TP + FP + FN} \quad (13)$$

All experiments were carried out using MATLAB (R2022a) on a PC with 11th Gen Intel® Core™ i5-11300H 3.11 GHz CPU and 16.0 GB RAM.

#### IV. EXPERIMENT AND RESULTS

##### A. Parameter Selection

Equal division was used for intra-beat segmentation. Each segment had 4-16 sample points, and the length of the feature sequence within one heartbeat ranged from 45-11. Since the feature sequence was restricted, the length of sequential pattern  $m$  was set to 2 to ensure the number of edges was substantially bigger than the number of nodes in the network.

The symbolic encoding threshold value was dynamically determined according to individual changes in ECG signal shape, such as amplitude. The peak value of the statistical property sequences in each pulse in the ECG record was set as  $\{P\}$ , and the minimum value was set as  $thr_1$ . The numerical distribution range in the set  $\{P\}$  was evenly divided into four sections, and the values at the three split points were the choices of  $thr_2$ , as shown by (14).

$$thr_1 = \min\{P\} \quad (14)$$

$$thr_2 = \min\{P\} + \alpha \times \frac{\max\{P\} - \min\{P\}}{4}, \alpha = 1, 2, 3 \quad (15)$$

The optimal number of learning cycles, or the number of individual classifiers that comprised the ensemble classifier, was determined by five-fold cross-validation when the number of intra-beat segments was provisionally set to 30 with the  $\alpha$  parameter set to 1. Fig. 3 (A) depicts the change in five-fold cross-validated F1 for PVC as a function of the number of learning cycles. According to these data, 150 learning cycles with a higher average F1 were chosen for subsequent investigations.

Fig. 3 (B) shows the classification performance on MIT-BIH-AR using ROS and a five-fold cross-validation technique with 45 to 11 intra-beat segments and varied thresholds  $thr_2$  (Parameter  $\alpha$  range from 1 to 3). The average AUC and F1

were optimal when the number of intra-beat segments was 30, each with 6 sample points, and  $\alpha$  was 1. Thus, these parameters were selected for following trials.

##### B. Transition networks mapping from ECG waveform

The features characterize the temporal dynamic information of the ECG signals by fully capturing the transition patterns attributed to the morphological changes, so that they are distinct for various types of heartbeats and have excellent interpretability. As depicted in Fig. 4, there is an intuitive tendency to distinguish the feature sequences and topologies of corresponding networks between the two categories. Moreover, the sequential patterns are closely associated with typical waveform segments, and through their interrelationship the dynamics of ECG waveform are reconstructed.

For the PVC type, the QRS complex acquires an anomalous morphology, such as enlarged and abnormal waveform. Due to higher amplitude, the rise and fall of the QRS complex change more rapidly, therefore corresponding to nodes '1-3' and '3-1' (Line D in Fig. 4). Whereas, the same part in normal beats changes gently compared to PVCs, more mapped to node '1-2' and '2-3' (Line B in Fig. 4). Consequently, node '1-3' or '3-1' suggest a major shift in ECG signal shape, and node '1-1' is related to the baseline and small waves. Meanwhile, the wide QRS complex in PVCs results in a wider spectrum of corresponding fluctuations in the feature sequences, including positive area, energy, average, ARV, and RMS. After symbolic encoding, the continuous symbol '3' appears more frequently in coarse-grained sequences, causing the sequential pattern '3-3' to appear more frequently, thereby increasing the degree of node '3-3' in the network. In most cases, PVC results in aberrant repolarization, manifesting as ST-segment and T-wave abnormalities. In record 119 of the MIT-BIH-AR, for instance, the occurrence of T-wave inversion resulted in an additional peak in the corresponding portion of each sequence, thereby forming a network with a more complex topology, as shown in Line E in Fig. 4. The appearance of more sequential patterns increases the connectivity of the network and changes the weight distribution. Occasionally, an irregularly descending QRS branch caused by PVC can also influence the feature sequences, particularly the negative area and its corresponding

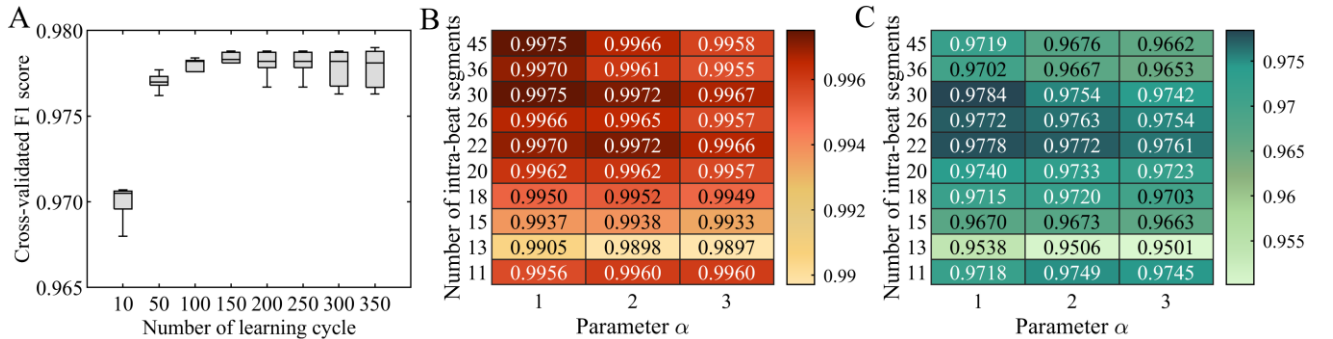


**Fig. 3.** Parameter selection for mapping ECG signals to transition networks. (A) Five-fold cross-validated F1 score for PVC plotted against the number of learning cycles in the ensemble classifier when the number of intra-beat segments was provisionally set to 30 and the  $\alpha$  parameter was set to 1. (B) Five-fold cross-validated average AUC and (C) Five-fold cross-validated average F1 plotted against the number of intra-beat segments and different thresholds.

&gt;&gt;

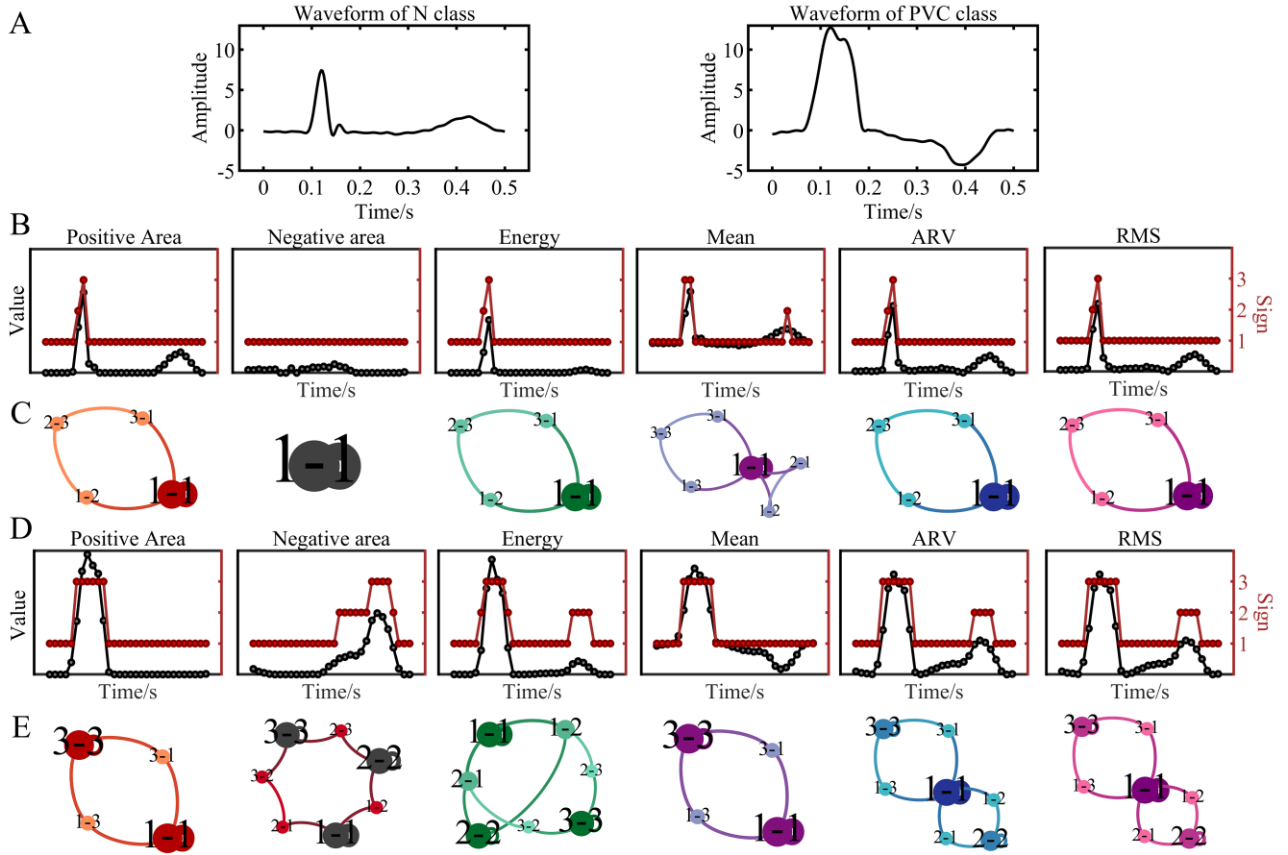


**Fig. 4.** The relationship between the heartbeat waveforms, feature sequences and corresponding transient networks. Line A: The waveforms of two heartbeat types (Taking record 119 in MIT-BIH-AR as an example). Line B: The six statistical property sequences corresponding to the N type heartbeat (left Y-axis) and the symbol sequences after symbolic encoding (right Y-axis). Line C: The transient networks mapped from the statistical property sequences of the N type heartbeat. The size and color of the nodes are set according to the order of the degrees. The larger the nodal degree, the larger the size and the darker the color. Line D: The six statistical property sequences corresponding to the PVC type heartbeat (left Y-axis) and the symbol sequences after symbolic encoding (right Y-axis). Line E: The transient networks mapped from the statistical property sequences of the PVC type heartbeat.

network topology.

The nodes in the network fully reveal the valuable information of the waveform. The higher nodal degree, the more frequent the sequential pattern appears, indicating the repeated occurrence of the corresponding waveform. Especially, the number of self-loop also reflects the duration in one pattern. Forbidden sequential patterns (sequential patterns cannot exist) have attracted attention from time series researchers [33], giving an area for future investigation.

### C. Results on the Three Independent Databases

Table II shows the classification performance of the proposed method on three databases. The five-fold cross-validation performance on MIT-BIH-AR was 0.9975 AUC, 0.9721 Se, 0.9848 P+, and 0.9784 F1, which was comparable to the sophisticated algorithms with outstanding classification performance [34-36]. The generalizability and classification performance were comprehensively assessed by testing on the INCART and WECG database with MIT-BIH-AR database as training dataset. The results on INCART database were 0.9887 AUC, 0.9611Se, 0.9656 P+ and 0.9633 F1, and on WECG database were 0.9755 AUC, 0.9517 Se, 0.9417 P+, and 0.9467 F1.

### D. The sensitivity of R-wave peak

R-wave peak accuracy impacts heartbeat feature extraction, especially for dynamic ECG data. Thus, a randomly distributed offset in a specified range was applied to the precise R-wave peak site to mimic R-wave detection errors. Training set was the MIT-BIH-AR and testing set was the WECG database with offsets from 0 ms to 150 ms with 50-ms increment.

Fig. 5 (A) shows that as R-wave peak offset increased, PVC AUC, Se, P+, and F1 dropped. When there was an R-wave peak offset within 50-ms, PVC Se was only reduced by 0.0054, whereas P+ decreased by 0.0815, lowering F1 and AUC to 0.9012 and 0.9719, respectively. When offset surpassed 50-ms, PVC P+ was considerably influenced. When offset increased from 50 ms to 100 ms, P+ decreased to 0.6256 and F1 dropped to 0.7521. When the offset range was 150-ms, Se decreased to 0.8781 with P+ reduced to 0.5998, making it more likely to misidentify the N type as PVC. The study [37] suggested that an offset within a 50-ms range around the R-wave peak was considered acceptable. In this condition, the experimental results demonstrated that the proposed algorithm exhibited a certain level of robustness to R-wave peak offsets.

&gt;&lt;

TABLE II  
THE RESULTS ON THE THREE DATABASES

Database	AUC	Se	P+	F1
*MIT-BIH-AR	0.9975 $\pm 1.41e^{-4}$	0.9721 $\pm 0.0016$	0.9848 $\pm 0.0012$	0.9784 $\pm 3.32e^{-4}$
INCART	0.9887	0.9611	0.9656	0.9633
WECG	0.9755	0.9517	0.9417	0.9467

\* The results on this database are expressed as the mean  $\pm$  standard deviation after five-fold cross-validation.

### E. The robustness against noise

The ECG records from MIT-BIH-NST were directly processed for heartbeat segmentation and feature extraction without filtering to assess the noise resistance of the proposed algorithm. Figure 5 (B) presents the categorization findings. The left side of each subplot displays the result of raw signal data to facilitate visual comparisons. It was observed that the classification performance was significantly affected by the SNR, particularly for the positive category (P+). When the SNR was 18 dB, indicating a relatively clean signal, the classification scores were found to be satisfactory. The AUC was above 0.9722, and the F1-score exceeded 0.941. Even at an SNR of 6 dB, where the noise power constituted 25% of the signal power, the algorithm still achieved acceptable results, with AUC and F1 above 0.9331 and 0.8289, respectively. These findings demonstrate that the algorithm is capable of maintaining reasonable classification performance even under low SNR conditions. In a worst-case scenario (results under noise ‘em’), the performance of the algorithm was negatively impacted. Specifically, the P+ for PVC dropped to 0.6449, and the Se decreased to 0.8483, resulting in an F1 reduction to 0.7327. However, despite this decline, the algorithm maintained high classification performance and exhibited resilience to noise, with AUC values consistently above 0.90 across four different noise levels. Among the various types of

noise investigated, electrode motion artifact was identified as the most influential. As the signal quality deteriorated due to this artifact, the classification performance notably worsened. This was evident from the decrease of 0.0154 and 0.0307 in AUC and F1, respectively, which were poorer compared to the best results obtained in the other three noise categories at an SNR of 3 dB.

Fig. 5 (C) depicts the classification outcomes for identifying PVCs on the ECG dataset during four different daily activities. With the increasing intensity of activity, the decreasing SNR led to a decline in classification results. There was little difference in the classification performance between sitting state and talking state, while the higher noise level during walking and jogging resulted in a reduction in F1 by 0.0117 and 0.0212, as well as a decrease of 0.0228 and 0.0289 in P+, respectively. Especially during jogging, Se dropped to 0.9287, indicating a weakened capability for PVC identification. Despite the influence of noise on classification performance, the most affected performance evaluation metric, P+, experienced only a modest reduction of 0.0289, highlighting the algorithm’s high robustness. Therefore, the test demonstrates that the algorithm efficiently meets classification requirements during daily activities.

### V. DISCUSSION

This paper presented a transition network-based noise-resistant PVC detection algorithm. The dynamic properties of a heartbeat were appropriately mapped into the network, therefore the topological metrics of the network representing ECG morphological dynamics were useful and necessary elements for categorization. This algorithm developed a unique way for capturing the dynamic properties of ECG signals with strong classification capacity for PVC identification in dynamic ECG data. The key findings in this paper are: (1) Good-interpretable features representing ECG temporal dynamics were identified and used in classification

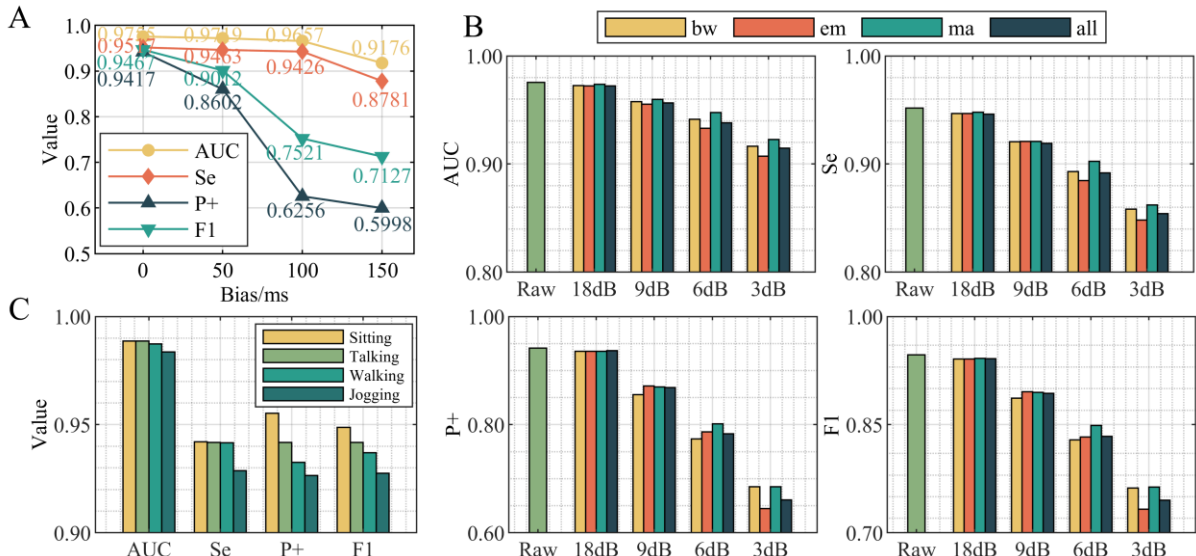


**Fig. 5.** The results of robustness tests. (A) The effect of R-wave location offset on classification results of the proposed method. (B) The effect of additional noise on classification results of the proposed method. (C) The test results on ECG dataset during four different daily activities.

&gt;&lt;

using nonlinear analysis of transition networks. (2) A noise-immune, R-wave peak offset-insensitive PVC detection technique was provided. (3) Multiple datasets proved this algorithm's classification and generalization abilities. (4) Applying transition networks to the classification of beat-to-beat arrhythmias. The method has high performance, minimal complexity, and quick processing, making it suitable for wearable device applications.

#### A. Comparison with Existing Algorithms

The exhaustive evaluation of the results on MIT-BIH-AR attained a level comparable to other current algorithms with high precision. Petryshak et al. [34] developed a PVC detection model, cooperating an inception U-Net network for R-wave peak detection and a CardioIncNet network for PVC recognition, which attained a cross-validation result of 0.964 F1. J. Yang et al. [35] proposed a novel deep learning model (ECGDet) for the detection of PVCs or supraventricular premature beats. For PVC detection, model achieved five-fold cross-validation classification results of 0.926 F1, 0.958 Se, and 0.920 P+. M. Hammad et al. [38] proposed a deep learning model (ResNet-LSTM network) that integrated with k-NN and genetic algorithm (GA) optimization for 5 types of arrhythmias classification, with a performance of 0.997 Se, 0.958 P+, and 0.897 F1. Despite the algorithm's capability to identify multiple arrhythmias, its PVC recognition accuracy was slightly lower compared to the method in this study (Se=0.957 and P+=0.917). Sarshar et al. [36] utilized a CNN-based deep learning network for PVC detection with 3 morphological features and 7 statistical features, outperforming the results of proposed method with 0.989 F1, 0.992 Se, and 0.986 P+. Although deep learning models are more likely to accomplish high-precision classification results, it is important to consider the algorithm's complexity and its compatibility to dynamic applications. Arrais Junior et al. [39] devised a real-time optimized PVC recognition algorithm based on redundant discrete wavelet transform (RDWT). This algorithm obtained substantial classification performance on the MIT-BIH-AR database, with 0.9918 Se and 0.9915 P+, with its low computational complexity. However, the frequency band distribution of RDWT in this algorithm was only performed at a sampling rate of 350Hz, and the classification performance of ECG signals with various sampling rates was not discussed or validated. In contrast, the proposed algorithm utilized a coarse-graining procedure based on symbolic dynamics, in which the sampling rate had negligible impact on the features and outcomes.

Meanwhile, the classification performance was verified on the INCART database to assess the generalizability of the proposed method, comparable with existing approaches. The PVC recognition algorithm proposed by Allami et al. [14] were also tested on the INCART database, with slightly lower results than the proposed method. Sokolova proposed a rule-based method [11] with a higher P+ and a lower Se compared with the proposed method. However, based on its performance on MIT-BIH-AR database, its results indicated that the rule-based method was sensitive to the individual differences in

ECG signals. Malik et al. [40] introduced a novel approach to detect ventricular ectopy beat via the distance to the median beat in the record, while their performance was susceptible to ECG signal quality and was a bit low in Se to PVCs. Oster et al. [41] introduced a switching Kalman filter approach to track several morphologies for manual annotation by a cardiologist, incorporating unknown (X-factor) to improve the performance, with F1 reaching 0.994. However, this method relies heavily on the accuracy of R-wave peak localization, limiting his application.

#### B. Interpretability Analysis

In the handcrafted feature-based methods, various fiducial features relevant to QRS complex and ECG morphology, such as onset and offset of P, QRS, and T waves, were generally utilized for identifying PVC beats [10-12, 14, 36]. These kinds of features visualize the morphology of the ECG waveform and are highly interpretable. However, they are obviously affected by the accuracy and standards for the detection of fiducial point location, which are susceptible to noise. Moreover, the limited set of features overlooks the valuable information pertaining to waveform dynamics and trends, such as the rate of change in QRS complex and T-wave. Although some studies [42] used the mathematic geometric concepts such as slopes and angles to supplement the details of the waveform changes, this method increases the number and complexity of the features and only captures the information for specified parts. In the proposed method, the sequences of statistical properties within each intra-beat segment, obtained through equal division of a single heartbeat, reflect the dynamic changes in the waveform without requirement of high accurate fiducial point detector. Transition networks are mapped from them, where sequential patterns make it easier to identify specific shapes in the waveform, such as node '1-3' corresponding to rapid rise in the waveform, node '1-2' and '2-3' corresponding to a slow rise. Therefore, the proposed method has a good interpretability. In the form of pattern transition information, the waveform dynamics within one cardiac cycle are fully preserved in the network topology, thereby capturing sufficient dynamic characteristics.

Some of studies [40, 43] introduced morphology features based on the distance or correlation coefficients between the tested heartbeat and the median beat or template beat. However, these interpretable features are easily influenced by inappropriate templates. Compared with the above ruled-based studies, the features extracted in this study are also consistent with expert rules. As one of the most obvious characteristics of PVCs, the duration of the QRS complex is significantly larger than that in a normal beat (>120 ms) [10]. This corresponds to a decrease in the degree (reduced importance) of node '1-1' in transition networks mapping from PVCs and an increase in the number of non '1-1' nodes and their degrees. Generally, the amplitude of QRS complex in PVCs is much smaller or higher than that in the normal beats [14]. This is reflected in the network topology by the increased importance of node '3-3' for taller PVCs and the presence of nodes with higher coding value in the network corresponding to their

&gt; &lt;

negative area sequences for smaller PVCs. The correlation between the extracted features and expert rules is crucial to ensure credibility in clinical applications. The interpretable features in this study maintain consistency with decision-making processes in the clinical environment, thereby enhancing the potential in practical applications.

### C. Execution Efficiency

The analysis of algorithm efficiency plays a key role, which evaluates the performance and practicality of the algorithm across diverse platforms. Aimed to access the performance in real-world scenarios, the comparison with the existing real-time algorithms was carried out as illustrated in Table IV. Table IV lists the run time as well as the platforms on which the algorithms were run, accompanied by the average run time per 1-s segment for a convenient comparison. Compared to the Hajeb-Mohammadalipour's algorithm [44], which also runs on the PC and uses machine learning for classification, the algorithm in this study has an advantage in terms of computational speed. Meanwhile, some of the algorithms proposed in the research [14, 45] show excellent performance on mobile/wearable devices. Although the proposed algorithm has shorter run time on PC platform compared to the aforementioned algorithms, it is important to recognize the unique challenges posed by resource-constrained environments (e.g., mobile and wearable devices). Therefore, there is a need to analyze and optimize the algorithm for its computational complexity and efficiency.

Employing different lengths of ECG segments as inputs, the computational efficiency of the algorithm was analyzed, which depicted its temporal performance across various data sizes. As the run time shown in Table IV, it is found that the run time in the network construction and feature extraction stage exhibited generally linear growth with the amount of input data, indicating a linear temporal complexity. As the amount of input data increased, a proportional rise in the run time in feature extraction stage was observed, thereby favorable to estimate the time consumption. Because the preprocessing stage includes multiple phases, especially the iterative processes involved in the R-wave peak detection, may introduce non-linear aspect to the run time as the results shown. Fortunately, this part accounts for a small percentage of the run time. With the increase of input data length, an overall increase in the proportion of the total run time for feature extraction stage was observed. This finding highlights the need to optimize the efficiency of network construction and feature extraction in the future, to better fit the real-time requirements of practical applications.

### D. Robustness Analysis

In practical PVC detection, signal preprocessing and R-wave peak detection have a significant effect on the extraction of features. Even if the appropriate method is used, noise and inaccurate R-wave peak localization still inevitably influence feature extraction. In certain situations, nonlinear analysis methods offer greater robustness and noise resistance

TABLE III  
COMPARISON BETWEEN THE PROPOSED METHOD AND OTHER ADVANCED METHODS

Study	Method	Class	Database	F1	Se	P+	AUC
Petryshak et al. [34]	inception U-Net CardioIncNet	2 (N, PVC)	MIT-BIH-AR	0.964	-	0.966	-
J. Yang et al. [35]	ECGDet	2 (non-PVC, PVC)		0.926	0.958	0.920	-
M. Hammad et al. [38]	ResNet-LSTM network, k-NN, GA	5 (N, S, V, F, Q)		0.897	0.997	0.958	-
*Sarshar et al. [36]	CNN	2 (non-PVC, PVC)		0.989	0.992	0.986	-
*Allami et al. [14]	Pan-Tompkin's algorithm, CFNN	2 (non-PVC, PVC)		0.982	0.987	0.978	-
Arrais Junior et al. [39]	RDWT	2 (non-PVC, PVC)		-	0.9918	0.9915	-
Alickovic et al. [46]	DTW, MSPCA, Random Forest	4 (N, APC, PVC, RBBB)		0.848 0.995 <sup>D</sup>	-	-	0.960 0.994 <sup>D</sup>
*Sokolova et al. [11]	Rules	2 (non-PVC, PVC)		-	0.827	0.8297	-
<b>Proposed method</b>	Pan-Tompkin's algorithm, Transition network, Gentleboost	2 (N, PVC)		0.9784	0.9721	0.9848	0.9975
*Sokolova et al. [11]	Rules	2 (non-PVC, PVC)		INCART	-	0.9287	0.9703
*Allami et al. [14]	Pan-Tompkin's algorithm, CFNN	2 (non-PVC, PVC)	-		0.939	0.956	-
*Malik et al. [40]	AdaBoost	2 (non-PVC, PVC)	0.9206		0.8893	0.9542	-
Oster et al. [41]	Switching Kalman filter with X-factor	2 (non-PVC, PVC)	0.994		0.991	0.9996	-
<b>Proposed method</b>	Pan-Tompkin's algorithm, Transition network, Gentleboost	2 (N, PVC)	0.9633		0.9611	0.9656	0.9887

\* marks the method using ECG morphological features.

<sup>D</sup> marks the results after using multiscale principal component analysis for denoising.

TABLE IV  
COMPARISON BETWEEN THE PROPOSED METHOD AND OTHER REAL-TIME METHODS

Study	Platform	Run Time	Average Time per 1-s segment
Hajeb-Mohammadalipour et al. [44]	Dell Precision T3600 computer with an Intel Xeon E5-2667 2.9 GHz processor using MATLAB R2017a	~1.124 s per 8-s segment	140.5 ms
Arrais Junior et al. [39]	- using MATLAB R2014a	61.2 s per 30-min record	34 ms
Allami et al. [14]	Samsung Galaxy J1 motherboard with a quad-core Cortex-A7 1.2 GHz CPU using Java software	2.1 s per 20-s segment	105 ms
Ran et al. [45]	Xilinx Zynq XC-7Z020 FPGA chip with two ARM Cortex-A9 processors and an Artix-7 FPGA	2.895 s per 10-s segment	289.5 ms
<b>Proposed method</b>	PC with 11th Gen Intel Core™ i5-11300H processor at 3.11 GHz with 16.0 GB RAM using MATLAB R2022a	0.276 s per 10-s segment ( $t_{pre}=0.08$ s, $t_{fea}=0.112$ s)	14 ms
		0.77 s per 1-min segment ( $t_{pre}=0.088$ s, $t_{fea}=0.603$ s)	
		9.63 s per 10-min segment ( $t_{pre}=3.76$ s, $t_{fea}=5.8$ s)	
		26.38 s per 30-min record ( $t_{pre}=6.89$ s, $t_{fea}=17.56$ s)	

$t_{pre}$  represents the run time in the preprocessing stage,  $t_{fea}$  represents the run time in the network construction and feature extraction stage.

than linear analysis methods. Some studies [24] have demonstrated that sequential partition is computationally simple and noise-resistant, which has led to its widespread use in the classification of time series.

Considering the interference of noise from the environment and the problem of inaccurate R-wave peak detection in practical application, the noise test and R-peak offset test were conducted. These evaluations revealed an admissible R-wave peak location error and permissible noise interference. As for the robustness against R-wave peak location error, the classification capability remained acceptable despite a 0.0036 decrease in AUC and a 0.0455 decrease in F1 when the R-wave peak offset was within the commonly permissible range of 50 ms [37]. As for noise immunity, the performance was almost unaffected by slight noise interference (18 dB), slightly degraded by noise (9 dB), still acceptable when the noise power was a quarter of the signal power (6 dB), and severely impaired when the noise power reached half of the signal power (3 dB). The classification results of proposed method were comparable to those of Alickovic et al. [46] using the popular DWT feature extraction method with multiscale principal component analysis denoising on the MIT-BIH-AR database, while outperforming their AUC of 0.9480 without denoising.

In the test results of ECG dataset during daily activities, the minimal difference between sitting state and talking state suggest that the algorithm exhibits good robustness to slight baseline wander and muscle artifact. As for walking and jogging, they are more likely to introduce noticeable baseline wander, muscle artifact, and electrode motion artifact due to body movement, as well as changes in breathing rate and depth. Relative to marked and low-frequency baseline wander, the greater challenge lies in handling the effect of intermediate or high-frequency noise, which overlaps with the frequency of the ECG signals. Addressing such noise, the coarse-graining process mitigates the impact of low-amplitude noise, resulting in a slightly improved performance in the classification of

dynamic ECG signals. While the obvious fluctuation and local spikes introduced by noise, that may locally distort or overwhelm the ECG waveform, are the primary factors contributing to slightly degraded classification performance during exercise.

Although all three kinds of noise affect ECG morphology and degrade classification results, the baseline wander and muscle artifact may be more robust. As shown in the normalized curves of the three noise types in Fig. 6, baseline wander is gentle and less likely to cause large abrupt shifts in the morphology within one heartbeat. Muscle artifact manifests as small fluctuations at a high frequency, while the sensitivity to small amplitude changes is reduced after symbolic encoding. However, electrode motion artifact, which arises from unstable electrode-skin contact, generally in the form of a low-frequency signal, fluctuating more obviously in amplitude. Hence, it has a greater impact on the performance, making the algorithm more sensitive to it.

#### E. Limitations

Although the proposed method obtains high classification accuracy, fast computational speed, strong robustness, and excellent generalization ability in detecting PVCs, there are

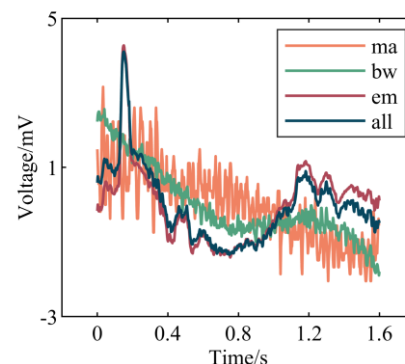


Fig. 6. Comparison of waveforms for the four types of noise signals after power normalization.

&gt;&lt;

still a number of potential limitations that need to be addressed. One limitation of this approach is the sensitivity to electrode motion artifact. As it is irregular in time and frequency, probably similar to the part of the spectrum of the ECG signals, so simple preprocessing does not completely remove its effects. Based on previous studies [47], independent component analysis combined with the proposed algorithm may be a good solution, which is able to extract the ECG from noisy signal. Furthermore, classification for PVCs in dilated cardiomyopathy was challenging when assessing patients with various health conditions. This difficulty stems from the enlargement of the QRS complex caused by dilated cardiomyopathy, resulting in a morphological similarity between PVCs and normal beats. In response to this limitation, incorporating non-morphological features can provide alternative characteristics of PVCs, enhancing the classification performance. It also leads to another constraint of this method, which is that only morphological features within one heartbeat were extracted, but the characteristics between beats were not utilized. Because the important rhythm information was ignored, the algorithm is more likely to be applied to arrhythmias with significant differences in morphology, e.g., premature atrial beats cannot be classified. In the future, the algorithm using hybrid features including network-based features and rhythm features will be developed for recognizing PVCs and more types of arrhythmias.

## VI. CONCLUSION

The study introduces a novel method for feature extraction and PVC detection based on the transition network approach. The proposed method was evaluated using three ECG databases, namely MIT-BIH-AR, INCART, and WECG. By employing this approach, interpretable characteristics that capture the comprehensive morphological dynamics of ECG signals were extracted. In addition, to further assess the classification performance in daily applications, our method was also tested under daily life conditions (sitting, talking, walking, and jogging). The experimental results demonstrate that the proposed method exhibits high computational efficiency, high PVC recognition accuracy and robustness and resilience to noise. These results highlight the potential of the proposed approach for practical applications, particularly for wearable mobile devices.

## VII. REFERENCES

- [1] World health statistics 2022: monitoring health for the SDGs sustainable development goals, World Health Organization, Geneva, Switzerland, 2022, Available: <https://apps.who.int/iris/handle/10665/356584>.
- [2] R. M. John *et al.*, "Ventricular arrhythmias and sudden cardiac death," *The Lancet*, vol. 380, no. 9852, pp. 1520-1529, 2012, DOI: 10.1016/S0140-6736(12)61413-5.
- [3] Y. Jin *et al.*, "A novel interpretable method based on dual-level attentional deep neural network for actual multilabel arrhythmia detection," *IEEE Transactions on Instrumentation and Measurement*, vol. 71, pp. 1-11, 2021, DOI: 10.1109/TIM.2021.3135330.
- [4] G. Engel *et al.*, "Prognostic significance of PVCs and resting heart rate," *Annals of Noninvasive Electrocardiology*, vol. 12, no. 2, pp. 121-129, 2007, DOI: 10.1111/j.1542-474X.2007.00150.x.
- [5] L. Parreira *et al.*, "Frequent premature ventricular contractions. Association of burden and complexity with prognosis according to the presence of structural heart disease," *Annals of Noninvasive Electrocardiology*, vol. 26, no. 1, p. e12800, 2021, DOI: 10.1111/anec.12800.
- [6] X. Peng *et al.*, "DSCSSA: A classification framework for spatiotemporal features extraction of arrhythmia based on the Seq2Seq model with attention mechanism," *IEEE Transactions on Instrumentation and Measurement*, vol. 71, pp. 1-12, 2022, DOI: 10.1109/TIM.2022.3194906.
- [7] B. Hou, J. Yang, P. Wang, and R. Yan, "LSTM-based auto-encoder model for ECG arrhythmias classification," *IEEE Transactions on Instrumentation and Measurement*, vol. 69, no. 4, pp. 1232-1240, 2019, DOI: 10.1109/TIM.2019.2910342.
- [8] L. Meng, K. Ge, Y. Song, D. Yang, and Z. Lin, "Long-term wearable electrocardiogram signal monitoring and analysis based on convolutional neural network," *IEEE Transactions on Instrumentation and Measurement*, vol. 70, pp. 1-11, 2021, DOI: 10.1109/TIM.2021.3072144.
- [9] X. Liu, H. Wang, Z. Li, and L. Qin, "Deep learning in ECG diagnosis: A review," *Knowledge-Based Systems*, vol. 227, p. 107187, 2021, DOI: 10.1016/j.knsys.2021.107187.
- [10] M. Hammad, A. Maher, K. Wang, F. Jiang, and M. Amrani, "Detection of abnormal heart conditions based on characteristics of ECG signals," *Measurement*, vol. 125, pp. 634-644, 2018, DOI: 10.1016/j.measurement.2018.05.033.
- [11] A. Sokolova, O. Markelov, M. Bogachev, and Y. D. Uljanitski, "Multi-parametric algorithm for premature ventricular contractions detection and counting," in *AIP Conference Proceedings*, 2019, vol. 2140, no. 1: AIP Publishing, DOI: 10.1063/1.5121999.
- [12] X. Chen, Y. Wang, and L. Wang, "Arrhythmia recognition and classification using ECG morphology and segment feature analysis," *IEEE/ACM Transactions on Computational Biology and Bioinformatics*, vol. 16, no. 1, pp. 131-138, 2018, DOI: 10.1109/TCBB.2018.2846611.
- [13] S. Raj and K. C. Ray, "ECG signal analysis using DCT-based DOST and PSO optimized SVM," *IEEE Transactions on Instrumentation and Measurement*, vol. 66, no. 3, pp. 470-478, 2017, DOI: 10.1109/TIM.2016.2642758.
- [14] R. Allami, "Premature ventricular contraction analysis for real-time patient monitoring," *Biomedical Signal Processing and Control*, vol. 47, pp. 358-365, 2019, DOI: 10.1016/j.bspc.2018.08.040.
- [15] Y. Zou, R. V. Donner, N. Marwan, J. F. Donges, and J. Kurths, "Complex network approaches to nonlinear time series analysis," *Physics Reports*, vol. 787, pp. 1-97, 2019, DOI: 10.1016/j.physrep.2018.10.005.
- [16] U. Parlitz, S. Berg, S. Luther, A. Schirdewan, J. Kurths, and N. Wessel, "Classifying cardiac biosignals using ordinal pattern statistics and symbolic dynamics," *Computers in Biology and Medicine*, vol. 42, no. 3, pp. 319-327, 2012, DOI: 10.1016/j.combiomed.2011.03.017.
- [17] M. McCullough, M. Small, H. Iu, and T. Stemler, "Multiscale ordinal network analysis of human cardiac dynamics," *Philosophical Transactions of the Royal Society A: Mathematical, Physical and Engineering Sciences*, vol. 375, no. 2096, p. 20160292, 2017, DOI: 10.1098/rsta.2016.0292.
- [18] T. Weng, J. Zhang, M. Small, R. Zheng, and P. Hui, "Memory and betweenness preference in temporal networks induced from time series," *Scientific Reports*, vol. 7, no. 1, p. 41951, 2017, DOI: 10.1038/srep41951.
- [19] A. L. Goldberger *et al.*, "PhysioBank, PhysioToolkit, and PhysioNet: components of a new research resource for complex physiologic signals," *Circulation*, vol. 101, no. 23, pp. e215-e220, 2000, DOI: 10.1161/01.cir.101.23.e215.
- [20] A. ECAR, "Recommended practice for testing and reporting performance results of ventricular arrhythmia detection algorithms," *Association for the Advancement of Medical Instrumentation*, vol. 69, 1987.
- [21] C. Liu *et al.*, "Signal quality assessment and lightweight QRS detection for wearable ECG SmartVest system," *IEEE Internet of Things Journal*, vol. 6, no. 2, pp. 1363-1374, 2018, DOI: 10.1109/JIOT.2018.2844090.
- [22] J. Pan and W. J. Tompkins, "A real-time QRS detection algorithm," *IEEE Transactions on Biomedical Engineering*, no. 3, pp. 230-236, 1985, DOI: 10.1109/TBME.1985.325532.
- [23] Z. Cai *et al.*, "Robust PVC Identification by Fusing Expert System and Deep Learning," *Biosensors*, vol. 12, no. 4, p. 185, 2022, DOI: 10.3390/bios12040185.
- [24] X. Sun, M. Small, Y. Zhao, and X. Xue, "Characterizing system dynamics with a weighted and directed network constructed from time

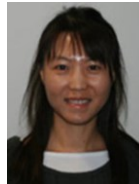
- series data," *Chaos: An Interdisciplinary Journal of Nonlinear Science*, vol. 24, no. 2, 2014, DOI: 10.1063/1.4868261.
- [25] X. Wang, X. Han, Z. Chen, Q. Bi, S. Guan, and Y. Zou, "Multi-scale transition network approaches for nonlinear time series analysis," *Chaos, Solitons & Fractals*, vol. 159, p. 112026, 2022, DOI: 10.1016/j.chaos.2022.112026.
- [26] L. Li, D. Alderson, W. Willinger, and J. Doyle, "A first-principles approach to understanding the internet's router-level topology," *ACM SIGCOMM Computer Communication Review*, vol. 34, no. 4, pp. 3-14, 2004, DOI: 10.1145/1015467.1015470.
- [27] I. Gutman, "The energy of a graph: old and new results," in *Algebraic Combinatorics and Applications: Proceedings of the Euroconference, Algebraic Combinatorics and Applications (ALCOMA), held in Gößweinstein, Germany, September 12-19, 1999*, 2001: Springer, pp. 196-211, DOI: 10.1007/978-3-642-59448-9\_13.
- [28] B. Ruhnau, "Eigenvector-centrality—a node-centrality?," *Social Networks*, vol. 22, no. 4, pp. 357-365, 2000, DOI: 10.1016/S0378-8733(00)00031-9.
- [29] A. Barrat, M. Barthelemy, R. Pastor-Satorras, and A. Vespignani, "The architecture of complex weighted networks," *Proceedings of the National Academy of Sciences*, vol. 101, no. 11, pp. 3747-3752, 2004, DOI: 10.1073/pnas.0400087101.
- [30] W. Lu, H. Hou, and J. Chu, "Feature fusion for imbalanced ECG data analysis," *Biomedical Signal Processing and Control*, vol. 41, pp. 152-160, 2018, DOI: 10.1016/j.bspc.2017.11.010.
- [31] A. Kubankova, D. Kubanek, and J. Prinosil, "Digital modulation classification based on characteristic features and GentleBoost algorithm," in *2011 34th International Conference on Telecommunications and Signal Processing (TSP)*, 2011: IEEE, pp. 448-451, DOI: 10.1109/TSP.2011.6043692.
- [32] J. Friedman, T. Hastie, and R. Tibshirani, "Additive logistic regression: a statistical view of boosting (with discussion and a rejoinder by the authors)," *The Annals of Statistics*, vol. 28, no. 2, pp. 337-407, 2000, DOI: 10.1214/aos/1016120463.
- [33] J. M. Amigó, S. Zambrano, and M. A. Sanjuán, "True and false forbidden patterns in deterministic and random dynamics," *Europhysics Letters*, vol. 79, no. 5, p. 50001, 2007, DOI: 10.1209/0295-5075/79/50001.
- [34] B. Petryshak, I. Kachko, M. Maksymenko, and O. Doboševych, "Robust deep learning pipeline for PVC beats localization," *Technology and Health Care*, vol. 29, no. S1, pp. 475-486, 2021, DOI: 10.3233/THC-218045.
- [35] J. Yang, W. Cai, and M. Wang, "Premature beats detection based on a novel convolutional neural network," *Physiological Measurement*, vol. 42, no. 7, p. 075003, 2021, DOI: 10.1088/1361-6579/ac0e82.
- [36] N. T. Sarshar and M. Mirzaei, "Premature Ventricular Contraction Recognition Based on a Deep Learning Approach," *Journal of Healthcare Engineering*, vol. 2022, 2022, DOI: 10.1155/2022/1450723.
- [37] H. Gao et al., "An open-access ECG database for algorithm evaluation of QRS detection and heart rate estimation," *Journal of Medical Imaging and Health Informatics*, vol. 9, no. 9, pp. 1853-1858, 2019, DOI: 10.1166/jmih.2019.2800.
- [38] M. Hammad, A. M. Iliyasa, A. Subasi, E. S. Ho, and A. A. Abd El-Latif, "A multitier deep learning model for arrhythmia detection," *IEEE Transactions on Instrumentation and Measurement*, vol. 70, pp. 1-9, 2020, DOI: 10.1109/TIM.2020.3033072.
- [39] E. Arrais Junior, R. A. d. M. Valentim, and G. B. Brandão, "Real-time premature ventricular contractions detection based on Redundant Discrete Wavelet Transform," *Research on Biomedical Engineering*, vol. 34, pp. 187-197, 2018, DOI: 10.1590/2446-4740.01618.
- [40] J. Malik, Z. Loring, J. P. Piccini, and H.-T. Wu, "Interpretable morphological features for efficient single-lead automatic ventricular ectopy detection," *Journal of Electrocardiology*, vol. 65, pp. 55-63, 2021, DOI: 10.1016/j.jelectrocard.2020.11.014.
- [41] J. Oster, J. Behar, O. Sayadi, S. Nemati, A. E. Johnson, and G. D. Clifford, "Semisupervised ECG ventricular beat classification with novelty detection based on switching Kalman filters," *IEEE Transactions on Biomedical Engineering*, vol. 62, no. 9, pp. 2125-2134, 2015, DOI: 10.1109/TBME.2015.2402236.
- [42] S. S. Al-Zaiti et al., "Machine learning for ECG diagnosis and risk stratification of occlusion myocardial infarction," *Nature Medicine*, vol. 29, no. 7, pp. 1804-1813, 2023, DOI: 10.1038/s41591-023-02396-3.
- [43] A. S. Malek, A. Elnahrawy, H. Anwar, and M. Naeem, "Automated detection of premature ventricular contraction in ECG signals using enhanced template matching algorithm," *Biomedical Physics & Engineering Express*, vol. 6, no. 1, p. 015024, 2020, DOI: 10.1088/2057-1976/ab6995.
- [44] S. Hajeb-Mohammadipour, M. Ahmadi, R. Shahghadami, and K. H. Chon, "Automated method for discrimination of arrhythmias using time, frequency, and nonlinear features of electrocardiogram signals," *Sensors*, vol. 18, no. 7, p. 2090, 2018, DOI: 10.3390/s18072090.
- [45] S. Ran et al., "Homecare-oriented ECG diagnosis with large-scale deep neural network for continuous monitoring on embedded devices," *IEEE Transactions on Instrumentation and Measurement*, vol. 71, pp. 1-13, 2022, DOI: 10.1109/TIM.2022.3147328.
- [46] E. Alickovic and A. Subasi, "Medical decision support system for diagnosis of heart arrhythmia using DWT and random forests classifier," *Journal of Medical Systems*, vol. 40, no. 4, p. 108, 2016, DOI: 10.1007/s10916-016-0467-8.
- [47] L. Xu et al., "Simulator of a full fetal electrocardiogram measurement chain by multichannel capacitive sensing," *IEEE Transactions on Instrumentation and Measurement*, vol. 69, no. 7, pp. 4348-4357, 2019, DOI: 10.1109/TIM.2019.2947979.



**Yumin Shen** received the B.S. degree in Measurement and Control Technology and Instrument from Southeast University, China, in 2021. She is currently pursuing the M.S. degree in the School of Instrument Science and Engineering, Southeast University, China. Her research interests include cardiac modeling, bio-signal processing, and network physiology.



**Zhipeng Cai** received the B.S. degree in Measurement and Control Technology and Instrument from Jiangsu University, China, in 2013. He obtained the M.S. and Ph.D. degree from Southeast University, China, in 2015 and 2019 respectively. He is currently receiving the Postdoctoral trainings and his research interests include bio-signal processing, intelligent monitoring system, and network physiology.



**Li Zhang** (Senior Member, IEEE) received the Ph.D. degree from the University of Birmingham, U.K., in 2004. She is currently a Reader in Royal Holloway, University of London, U.K. Her research interests include deep learning, intelligent robotics, and image processing. She has served as an Associate Editor for Decision Support Systems.



**Bor-Shyh Lin** (Senior Member, IEEE) received the Ph.D. degree from National Taiwan University, Taiwan, in 2006. He is currently a Professor with the Institute of Imaging and Biomedical Photonics, National Chiao Tung University. His current research interests include biomedical circuits and systems, biomedical signal processing, and biosensor.



**Jianqing Li** received the Ph.D. degree in Measurement Technology and Instruments in Southeast University. He is currently a Professor and Vice Present in Nanjing Medical University, China. He is also a Professor with the School of Instrument Science and Engineering, Southeast University, China. His research topics include wearable medical device and wireless network.



**Chengyu Liu** (Senior Member, IEEE) received the Ph.D. degree from Shandong University, China, in 2010. He is currently a Professor and the Dean of School of Instrument Science and Engineering, Southeast University, China. His research topics include mHealth and intelligent monitoring, machine learning and big data processing for cardiovascular signals, device development for CADs, sleep and emotion monitoring.